

Strange-attractor-driven matter

R. N. Valani¹ and D. M. Paganin²

¹*School of Mathematical Sciences, University of Adelaide, South Australia 5005, Australia*

²*School of Physics and Astronomy, Monash University, Victoria 3800, Australia*

(*Electronic mail: rahil.valani@adelaide.edu.au)

(Dated: 1 June 2025)

Strange attractors can arise from nonlinear dynamical systems, however, such attractors may also be used to drive complex dynamics. We outline a flexible deterministic formalism for such chaos-driven dynamics. By using a strange attractor to model each particle's internal state space, we present a new class of matter coined "strange-attractor-driven matter". As an illustrative example, we show how the strange-attractor-driven matter can be used for modeling dynamics and collective behavior reminiscent of active matter. This leads to a flexible model that can be used to generate a variety of active particle motions, for example run-and-tumble and run-reverse-flick motions, as well as more exotic motions such as curlicued trajectories with continuously-changing direction induced by a Lorenz attractor. When combined with particle interactions, these strange-attractor-driven particles gives rise to several characteristic active-matter phenomena such as clustering, jamming and flocking. In addition, the presented model enables active control over the motion of emergent clusters, with complex flocking features such as fusion, splitting and collisions of flocks emerging spontaneously. Beyond the illustrative example of active matter, the formalism of strange-attractor-driven dynamics presented in this paper may be applicable more broadly, to model complex dynamical and emergent behaviors in a variety of contexts.

Strange attractors emerge in the phase space of nonlinear deterministic systems exhibiting chaos. By coupling the spatial dynamics of a particle with a strange attractor associated with its internal state-space, we present a formalism to generate a new class of matter coined "strange-attractor-driven matter". We illustrate the rich dynamical and emergent behaviors arising from such particles by applying the formalism to generate phenomena reminiscent of active matter. The presented formalism provides a flexible way to generate complex dynamical and collective behaviors that may be applied broadly in various contexts.

walker, upon each bounce, generates a localized slowly decaying standing wave. The walker then interacts with these self-generated waves on subsequent bounces to propel itself horizontally. At high vibration accelerations, the waves created on each bounce decay very slowly in time and the walker's motion is not only influenced by the wave created on its most recent bounce, but also by the waves it created in the distant past, giving rise to memory in the system. In the high-memory regime, walkers mimic several peculiar features that were previously thought to be exclusive to the quantum realm³. An idealized theoretical model that captures the key dynamics of a walking droplet results in the following integro-differential trajectory equation⁴⁻⁶:

I. INTRODUCTION

In classical physics, objects are often modeled as point particles and the evolution of a single particle or a collection of interacting particles is governed by Newton's second law. In such dynamical systems, particles may be driven by deterministic forcing but their motion can exhibit chaos if nonlinearities are present. When a large number of variables are involved, it becomes impractical to evolve the entire system in time and sometimes the action of a large number of variables is replaced by "noise" resulting in stochastic dynamical systems. For example, Brownian motion of a small particle in a fluid may be described by a stochastic differential equation. In this paper, we take an alternative point of view, by presenting a class of particles that are driven by a strange attractor.

Before explaining strange-attractor-driven matter in any further detail, let us motivate such particles based on our observations associated with a system of walking droplets. Walking droplets^{1,2}, also known as walkers (or superwalkers), are a fascinating hydrodynamical system. In this system, millimetric droplets walk horizontally while bouncing vertically on the surface of a vertically vibrating liquid bath. The

$$\kappa \ddot{x} + \dot{x} = \frac{\beta}{2} \int_{-\infty}^t \sin(x(t) - x(s)) e^{-(t-s)} ds. \quad (1)$$

This dimensionless equation of motion describes one-dimensional horizontal dynamics of a walker located at x , which continuously generates waves with cosine-function spatial form that decay exponentially in time. The left side comprises an inertial term $\kappa \ddot{x}$ and a drag term \dot{x} . The right side quantifies the forcing on the droplet due to the underlying wave field, which is proportional to the gradient of the underlying field. Since this model takes into account the waves generated from all previous impacts, the underlying wave field is calculated through integration of waves generated from all the previous bounces of the walker. The two parameters, κ and β , may be interpreted as the ratio of inertia to drag and the ratio of wave forcing to drag respectively.

Valani *et al.*⁶ showed that the walker's integro-differential equation of motion in Eq. (1) can be transformed to the following system of ordinary differential equations (ODEs) (see

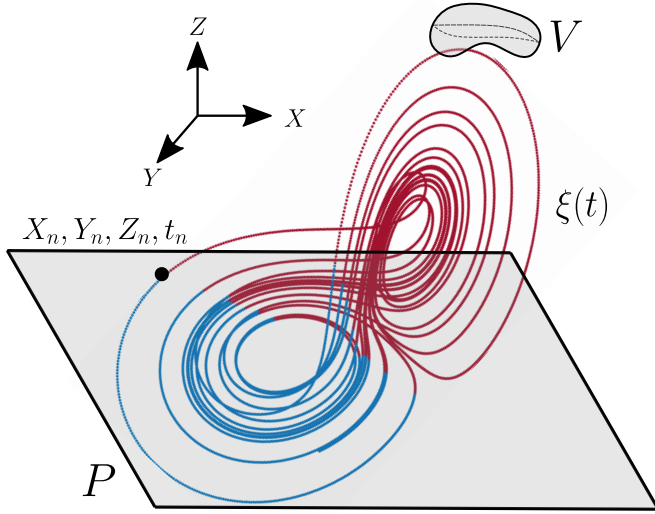


FIG. 1. Evolution of the state-space trajectory $\xi(t) = (X(t), Y(t), Z(t))$ along the strange-attractor set induces trigger times t_n such that $\xi(t_n) \in P$ or $\xi(t_n) \in V$, where P is a specified plane and V is a specified volume. The induced trigger times t_n , together with N arbitrary functions $f_j(t_n, \xi(t_n), \dot{\xi}(t_n), \ddot{\xi}(t_n), \dots)$, $j = 1, \dots, N$ of the strange-attractor trajectory at the trigger times, drive the spatio-temporal evolution of our strange-attractor-driven particle model.

Appendix A for a derivation):

$$\begin{aligned} \dot{X} &= X, \\ \dot{X} &= \sigma(Y - X), \\ \dot{Y} &= -XZ + rX - Y, \\ \dot{Z} &= XY - bZ. \end{aligned} \quad (2)$$

These ODEs are the classic Lorenz equations⁷ coupled with the droplet position. The X variable in the Lorenz system is equivalent to the droplet's velocity \dot{x} while the Y and Z variables are related to the memory forcing. The parameters σ, r, b in the Lorenz system are related to the walker's system via

$$\sigma = 1/\kappa, \quad r = \beta/2, \quad b = 1.$$

Thus, the walker's motion can be interpreted as being *driven* by the velocity X , which is evolving on the Lorenz strange attractor.

Inspired by this driving of a particle from an induced Lorenz strange attractor in the walking-droplet system, in this paper we present a general class of particles and the resulting matter, where each particle is coupled to a strange attractor arising from an internal state space of a low-dimensional chaotic dynamical system.

The paper is organized as follows. In Sec. II, we provide a flexible formalism for generating particles using strange attractors. In Sec. III, we provide an illustrative example of applying our strange-attractor-driven particles to generate behaviors reminiscent of active matter. We discuss some broader

implications of our paper, together with some possible avenues for future work, in Sec. IV. We offer some concluding remarks in Sec. V.

II. GENERAL METHOD TO GENERATE PARTICLE MOTION FROM STRANGE ATTRACTORS

We start by proposing a general method to generate a particle's dynamics using a governing strange attractor. As shown in Fig. 1, consider a general strange attractor of a chaotic dynamical system. A typical phase-space trajectory $\xi(t)$ evolves on this strange attractor. We consider an arbitrary plane P that cuts through this strange attractor or an arbitrary volume element V that has a non-zero measure of the strange attractor enclosed within it. Let t_n be the times when the trajectory on the strange attractor intersects the plane P or enters the volume element V for the n th time. We use these times t_n as trigger events for the particle. Such triggers could then be used to employ a measurable of the chaotic attractor at the trigger event to select the corresponding variable of the particle after the trigger event.⁸ For example, the trigger can be used to change the direction of motion of the particle, where the new direction of motion at time t_n may be a function of (i) the angle between P and the tangent to $\xi(t)$ at $t = t_n$, or (ii) the curvature of $\xi(t_n)$ at P , or (iii) the time spent within the state-space volume V , etc. In this way, one can construct a broad class of generic particle motions, driven by a strange attractor in an entirely deterministic manner. In the next section, we will provide specific examples of 1D and 2D strange-attractor-driven particles and the corresponding matter arising from their interactions in the context of active matter.

III. ACTIVE MATTER FROM STRANGE-ATTRACTOR-DRIVEN PARTICLES

Active matter refers to a large collection of active particles where each individual particle is a self-propelled entity that consumes energy from its surroundings and converts it into directed motion. Examples of active particles include motile living organisms such as humans, birds, fish or microorganisms such as sperm cells, bacteria and algae, as well as artificial autonomous entities such as active colloidal particles⁹, micro-robots¹⁰ and walking droplets^{1,2}. Active matter exhibits emergent collective phenomena such as bird flocks, mammalian herds, fish schools, insect swarms, bacterial colonies, swarming robots^{11–13}, motility-induced phase separation (MIPS) in active colloids¹⁴ and self-organization of microtubules and motors^{15,16}.

Complex locomotion of an individual active particle is typically modeled using a stochastic description. For example, a common minimal active-particle model is run-and-tumble particle (RTP) motion, also known as persistent diffusion¹⁷ or dichotomous diffusion¹⁸. Here, in one dimension, the overdamped stochastic dynamics of the active particle is governed by the Langevin equation¹⁹

$$\dot{x}(t) = u \sigma_s(t),$$

where an overdot denotes differentiation with respect to time t , x is the position of the active particle, u is a constant self-propulsion speed and $\sigma_s(t)$ is a dichotomous Markov noise term that flips between -1 and $+1$, following a constant-rate Poisson process. In two dimensions, the RTP “runs” at constant speed in a fixed direction and then instantaneously “tumbles”, i.e. reorients itself by choosing an angle randomly and isotropically^{20,21}. Such RTPs undergo ballistic motion over short times, while diffusive motion emerges at long times¹⁷. Two other widely used minimal models of active particles are Active Brownian particles (ABPs)²² and Active Ornstein-Uhlenbeck particles (AOUPs)²³.

Although a stochastic description is the norm for modeling the motion of active particles, there are examples of animate and inanimate self-propulsion systems where the motion of the active particle is generated from underlying low-dimensional chaotic dynamics, either explicitly or implicitly. Some of these examples include movement patterns of ants²⁴ and mud snails²⁵, locomotion of amoebas²⁶ and worms²⁷, active droplets²⁸, autonomous mobile robots^{29–32} and walking droplets^{33,34}. Moreover, features of active particle motion similar to random walks and diffusive behavior, can also emerge from deterministic chaotic processes. For example, several investigations have documented Brownian-like motion from deterministic dynamics^{35–40}. These models include the motion of a particle subjected to a deterministic but chaotic force. Deterministic diffusive motion also arises in Lorenz-like dynamical systems⁴¹ as well as in systems of delay differential equations^{42,43}. Recently, deterministic diffusion was observed in simulations of walking droplet dynamics governed by an integro-differential equation of motion^{5,6,44–47}.

Typically, when one models particle dynamics, the manifold of accessible states in the internal state space of that particle is topologically simple. For example, in conventional models of active matter, the structureless active particle is prescribed a constant self-propulsion velocity. This steady self-propulsion velocity for the entity being modeled, typically emerges from periodic internal processes that can be attributed to the entity. For example, periodically flapping wings of a bird give rise to its steady flying motion, periodic leg movements in a human give rise to steady walking motion and periodic beating of flagella gives rise to steady swimming for microorganisms. Moreover, the more complex locomotion patterns arising from unsteady movements of active entities are modeled using stochastic descriptions in conventional active matter models. For example, the complex trajectories of certain animals during foraging that may arise from complex internal processes is typically modeled using Lévy flights⁴⁸, or the complex interaction of a colloidal particle or a microorganism with the surrounding fluid medium is modeled as Gaussian white noise in ABPs⁴⁹. Here, we adopt an alternate viewpoint of modeling the internal complexity of an active particle via a strange attractor internal state-space (see Fig. 2) and exploring the resulting dynamics and emergent behaviors.

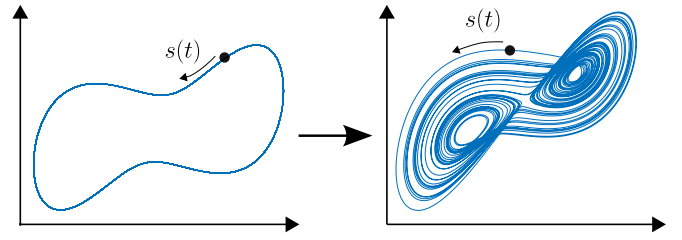


FIG. 2. Transition from (left) a topologically simple manifold of accessible states in the internal state-space of a particle (e.g. a limit cycle) to (right) a strange-attractor manifold of accessible points in the internal state-space of a particle, as considered in this paper. Here, $s(t)$ is a generalized coordinate (e.g. arc length) that may be attributed to the internal state-space degree of freedom.

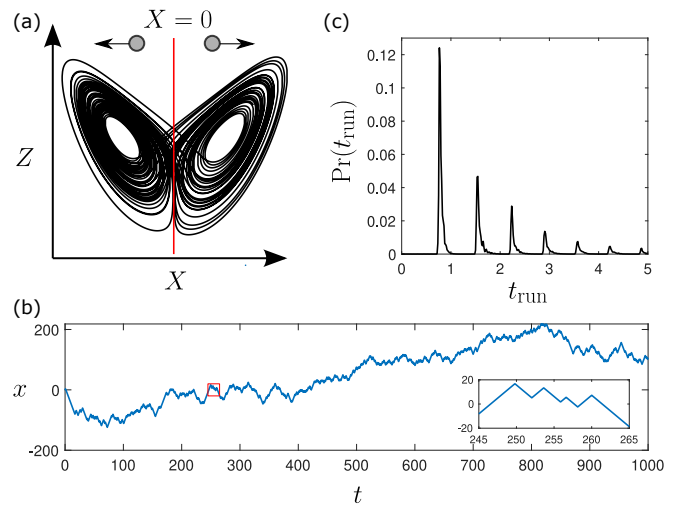


FIG. 3. One-dimensional deterministic RTP-like motion of an active particle driven by the Lorenz strange attractor. (a) The Lorenz attractor with parameters $\sigma = 10$, $r = 28$, $b = 8/3$ drives an active particle moving in one-dimension with a constant speed $u = \sqrt{r-1} = 3\sqrt{3}$. The active particle reverses its walking direction when the state-space trajectory on the attractor crosses the $X = 0$ cutting plane. (b) Typical space-time trajectory. (c) Probability distribution of time spent in constant-speed ballistic motion between direction reversals.

A. Strange-attractor-driven active matter in 1D

1. Single active particle

We start by applying the formalism presented in Sec. II to generate a one-dimensional RTP-like active particle motion. The RTP in one-dimension has been studied extensively^{50–55}. We here generate RTP-like motion in one dimension using the Lorenz strange attractor. We coarse-grain the system in Eq. (2) by only considering the sign of X for the first equation,

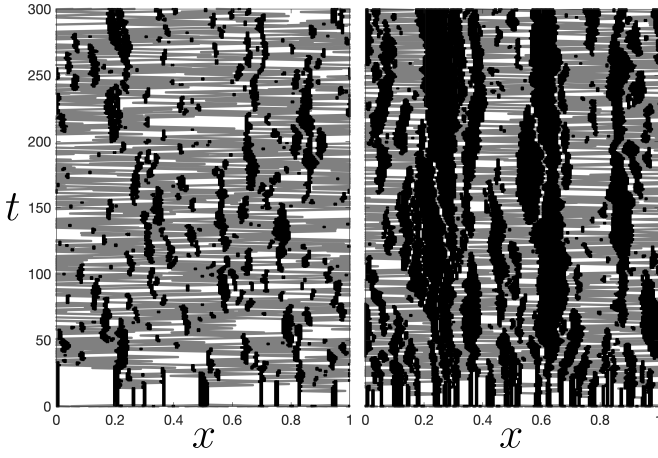


FIG. 4. Interactions of many Lorenz-attractor-driven 1D active particles on the unit interval with periodic boundary conditions. Upon addition of excluded-volume interactions (see Appendix B) in the Lorenz-attractor-driven active particles described in Fig. 3 with $u = 0.2$, we see the emergence of clustering and jamming. Space-time trajectories show the development of small-scale short-lived clusters for 50 particles (left), while long-lived large clusters emerge for 100 particles (right). The gray trajectories denote isolated particles while the black trajectories denote clusters. The size of each particle is 0.005.

giving

$$\begin{aligned}\dot{x} &= u \sigma_d(X), \\ \dot{X} &= \sigma(Y - X), \\ \dot{Y} &= -XZ + rX - Y, \\ \dot{Z} &= XY - bZ.\end{aligned}\tag{3}$$

Here, $\sigma_d(X) = \text{sgn}(X)$ and u is a constant denoting the self-propulsion speed of the active particle. This gives rise to one-dimensional RTP-like dynamics where the particle runs to the left or the right with a constant speed u and switches direction when the sign of the variable X flips, i.e. when a trajectory on the Lorenz strange attractor switches basin of attraction (see Fig. 3(a)).

Figures 3(b)-(c) show a typical space-time trajectory and the corresponding probability distribution of run durations for this Lorenz-attractor-driven particle. For a conventional RTP driven by a Markov dichotomous process, the run durations between direction changes are exponentially distributed¹⁸. However, for the RTP generated via our Lorenz-attractor-driven model, the distribution of run durations is inherent to the attractor and here results in a distribution with spikes at discrete time intervals, having an exponential decay envelope (see Fig. 3(c)). These spikes emerge because once the particle switches from one basin of the attractor to another, it performs a discrete number of orbits in that basin, before switching basins again. We highlight that the characteristic elements of the underlying chaotic flip-flop motion between the two wings of the Lorenz attractor are imprinted on this probability distribution of run durations.

The probability distribution of run durations in our strange-attractor-driven active particle model can be fixed by the un-

derlying strange attractor or allowed to freely evolve, e.g. by (i) evolving the parameters σ, r, b of the driving Lorenz system at each trigger event, in a manner governed by the state-space trajectory at each such event, or (ii) leaving the driving attractor fixed but changing the process of triggering the particle's direction change by evolving the cutting plane P in Fig. 1 in a manner that is deterministically driven by the state-space trajectory at each trigger event.

Our simple formalism employed with different strange attractors can generate a wide variety of active particle motion in one-dimension. For example, one can use this formalism to generate conventional active particle motion such as ABP-like motion and AOUP-like motion, as well as different kinds of active particles with anomalous distributions of run durations (see Appendix C).

2. Many interacting active particles

We now turn to the question of emergent behavior, in the context of our formalism. Emergent behavior is a feature of active-matter systems, that arises when interactions are encoded at the level of individual active particles. For example, in one-dimension, interaction of many RTPs with purely repulsive excluded-volume interactions results in clustering and jamming^{56–58}, while introducing simple aligning rules gives rise to one-dimensional flocking states that can stochastically change direction⁵⁹. Moreover, interactions induced by a purely repulsive potential can give rise to motile and dynamic clusters for various kinds of active particles in one-dimension⁶⁰. We can readily include repulsive interactions in our 1D strange-attractor-driven RTPs. For example, Fig. 4 shows spatiotemporal plots of many interacting 1D Lorenz-attractor-driven active particles (described in the caption to Fig. 3), coupled via an added excluded-volume interaction, with the system being confined on the unit interval with periodic boundary conditions. We see the emergence of clustering and jamming. For smaller numbers of particles we observe short-lived small clusters. Increasing the particle density leads to longer-lived larger clusters. By including short-range spring-like interactions we also obtain dynamic and motile clusters, while introducing aligning interactions results in flocking states that intermittently reverse direction (see Appendix C).

In addition to generating emergent behaviors similar to those realized in conventional active-matter models, our strange-attractor-driven active matter formalism also allows us to readily control and manipulate the emergent behaviors, via relatively simple modifications to the underlying strange attractor driving. For example, as shown in Fig. 5(a), if the cutting plane for each particle is translated to

$$X = k > 0,\tag{4}$$

then each particle will on average spend more time traveling to the left. Hence, when a cluster is formed, particles are more likely to leave the left side of that cluster and also more likely to join the right side of an adjacent cluster. This results in a net drift of clusters to the right. Thus, by a simple translation of

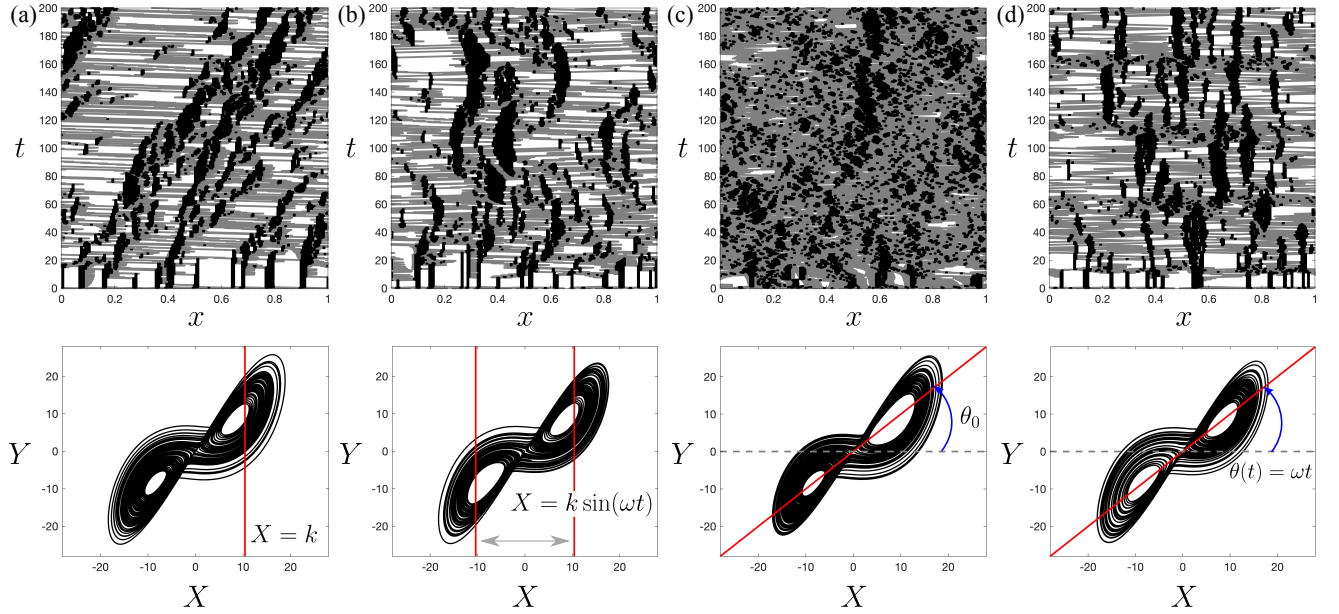


FIG. 5. Various emergent behaviors arising for a collection of 50 interacting 1D Lorenz-attractor-driven active particles (top panels) by making simple modifications to the strange attractor driving (bottom panels). (a) Offsetting the cutting plane of each active particle to $X = k$, where $k = 2\sqrt{r} - 1$, results in drift of the emergent clusters. (b) Choosing an oscillating cutting plane for each particle of the form $X = k \sin(\omega t)$, with $\omega = 2\pi/100$, results in oscillations of the emergent clusters. (c) Changing the cutting plane for each particle to $Y = \tan(\theta_0)X$, with $\theta_0 = \pi/4$, gives rise to a different type of clustering with dominance of short-lived small clusters. (d) Allowing the cutting plane to rotate according to $Y = \tan(\omega t)X$, with $\omega = 2\pi/100$, results in periodic formation and disintegration of clusters. All other parameters are the same as those employed in Fig. 4.

the cutting plane for the Lorenz-attractor-driven particle, one can induce a desired drift in the emergent clusters. Position dependence of this cutting-plane, namely a cutting-plane field $P(x)$ described by

$$a(x)X + b(x)Y + c(x) = 0 \quad (5)$$

with a, b, c being arbitrary functions of x , will enable one to introduce an induced potential landscape in which the clusters' drift direction and speed varies with spatial position x . This particular generalization, while interesting, will not be further considered at this point. Rather, we now explore how time dependence in the position of the cutting plane can be used to control the motion of the clusters. For example, if the cutting plane is allowed to oscillate between $X = k$ and $X = -k$, then this will induce an oscillation in the cluster dynamics as shown in Fig. 5(b). Instead of choosing a vertical cutting plane in the (X, Y) projection of the attractor, if the cutting plane is inclined at an angle $\theta_0 = \pi/4$, then the dynamics of emergent clusters and their size distribution changes significantly (see Fig. 5(c)). At the angle shown in Fig. 5(c), one obtains short lived smaller clusters due to frequent crossing of the inclined cutting plane by the phase-space trajectory. This changing cluster distribution for the cutting plane at different angles can be exploited to model complex clustering behaviors. For example, allowing the cutting plane to rotate in a periodic manner, one can induce periodic formation and disintegration of clusters as shown in Fig. 5(d).

We highlight that in all of these examples, the characteristics of the underlying Lorenz attractor are imprinted in the

cluster dynamics and the cluster size distribution, and if the underlying attractor is changed then the corresponding emergent cluster dynamics and statistics will change accordingly.

B. Strange-attractor-driven active matter in 2D

1. Single active particle

We now extend this formalism to two spatial dimensions. As an indicative example, in 2D the x and y spatial coordinates of the particle may be taken to evolve via

$$\dot{\mathbf{x}} = (\dot{x}, \dot{y}) = (u \cos(\theta(t)), u \sin(\theta(t))).$$

Here, u is a constant speed and the angle $\theta(t)$ is now a dynamical variable linked to a strange attractor. We construct 2D strange-attractor-driven active particles whose distribution of run durations is dictated by the choice of the cutting plane and the underlying attractor, and the turning angles $\Delta\theta_n$ are determined by the choice of a measurable of the underlying attractor at the trigger times t_n . For the Lorenz strange attractor with $X = 0$ as the cutting plane, we can choose the turning angle in various ways. For example, choosing

$$\Delta\theta_n = Z(t_n) \bmod(2\pi)$$

results in a nearly uniform distribution of turning angles. A typical trajectory generated in this manner and the corresponding turning-angle distribution are shown in Figs. 6(a)-

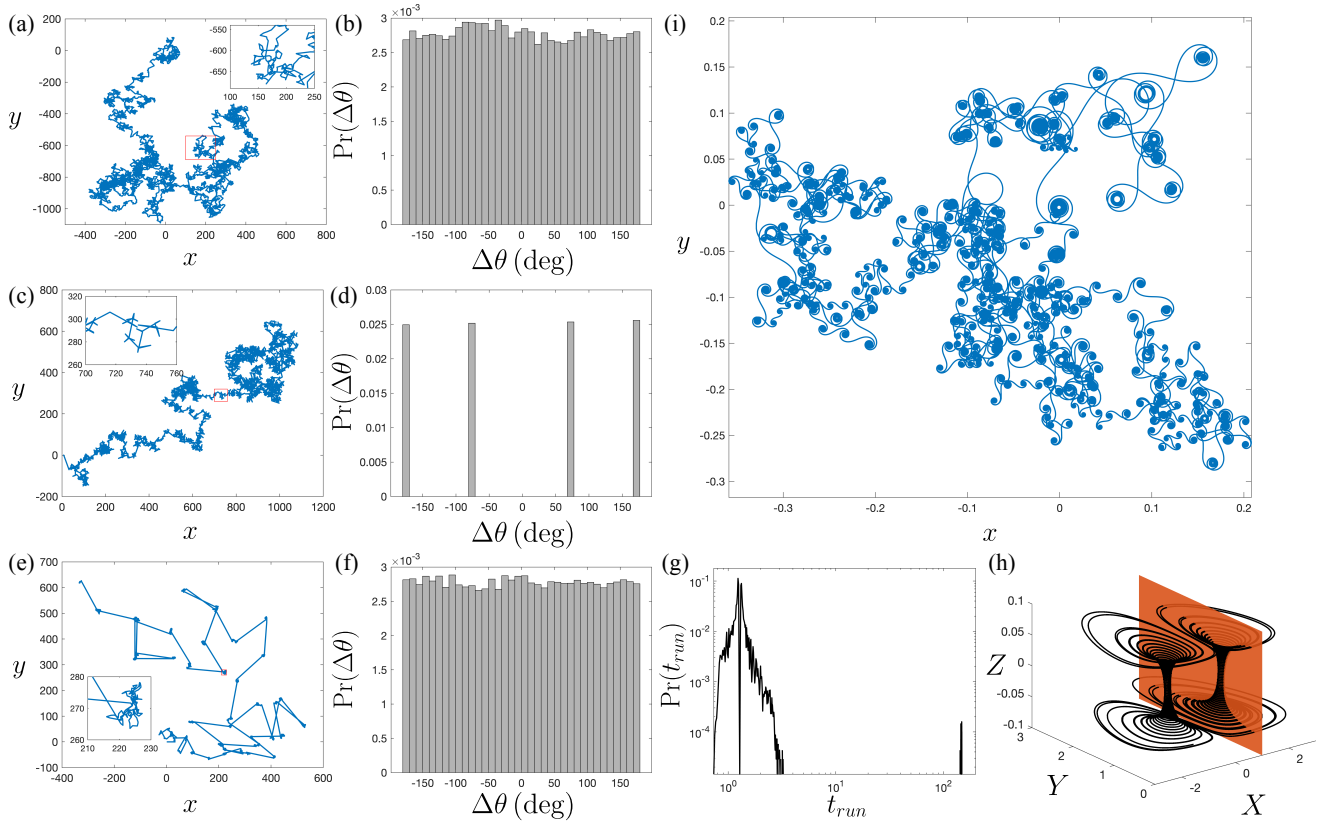


FIG. 6. Two-dimensional strange-attractor-driven active particle motions. (a) A 2D RTP-like active particle trajectory generated from the Lorenz system with parameters $\sigma = 10$, $r = 28$, $b = 8/3$ and self-propulsion speed $u = \sqrt{r-1}$. The cutting plane is $X = 0$, which results in a run length distribution that is the same as Fig. 3(c). The turning angles are chosen as $\Delta\theta_n = Z(t_n) \pmod{2\pi}$, with the trigger times t_n , resulting in a nearly uniform turning angle distribution as shown in panel (b). (c) Active particle driven in the same way as in (a) except that (d) turning angles are prescribed to alternate between $\pm\Delta\theta_1 = 71^\circ$ and $\pm\Delta\theta_2 = 176^\circ$ to mimic run-reverse-flick motion. (e) An intermittent active particle trajectory generated from the Bouali attractor⁶¹ ($\dot{X} = 3X(1-Y) - 2.2Z$, $\dot{Y} = -(1-X^2)Y$, $\dot{Z} = 0.001X$ with $X = 1$ as the cutting plane and self propulsion speed $u = 1$) where the particle alternates between a “long run” phase of ballistic motion and an “explore” phase of diffusionlike motion. For this trajectory, (f) shows the deterministically generated uniform turning-angle distribution, (g) shows the probability distribution of time spent in ballistic motion between direction changes on a logarithmic scale highlighting the two separate time scales, and (h) shows the Bouali attractor along with the cutting plane (red). (i) Active particle driven in the same way as in (a) but the turning angles are updated continuously at each instant of time according to $\Delta\theta(t) = Z(t) \pmod{2\pi}$, resulting in an exotic curlicued trajectory with long-time diffusionlike motion.

(b). This 2D RTP-like active particle undergoes ballistic motion at short times and diffusivelike motion at longer times.

Instead of determining the turning angles directly from the strange attractor, one can also construct a trajectory based on a prescribed probability distribution of turning angles. For example, we can generate run-reverse-flick-like motion by alternating between two different turning angles. We choose the turning angle to be $\pm\Delta\theta_1$ at trigger times t_{2k} and $\pm\Delta\theta_2$ at trigger times t_{2k+1} , where k is any natural number. We simulate two different trajectories on the driving Lorenz strange attractor at the same parameter values but different initial conditions. This results in the evolving trajectories

$$\begin{aligned}\xi_0(t) &= (X_0(t), Y_0(t), Z_0(t)), \\ \xi_1(t) &= (X_1(t), Y_1(t), Z_1(t)).\end{aligned}$$

When the trajectory $\xi_0(t)$ hits the plane $X_0 = 0$, it acts as a trigger to cease the run phase and choose a turning angle ac-

cording to

$$\Delta\theta = \frac{1}{2} \text{sgn}(X_1) \left[(\Delta\theta_2 - \Delta\theta_1) \text{sgn}(X_0) + (\Delta\theta_2 + \Delta\theta_1) \right].$$

By choosing $\Delta\theta_1 = 71^\circ$ and $\Delta\theta_2 = 176^\circ$, we obtain a trajectory similar to run-reverse-flick motion of bacteria⁶², as shown in Fig. 6(c)-(d). We can also use the trigger times t_n to generate arbitrary turning-angle distributions (see Appendix D).

Using different strange attractors we can generate active-particle trajectories of different types. For example, Fig. 6(e) shows an intermittent active particle trajectory generated using the Bouali attractor⁶¹ with a deterministically generated uniform turning angle distribution based on trigger times t_n using the method in Appendix D (see Fig. 6(f)). Here the particle alternates between phases of a long “run”, where it undergoes long time ballistic motion, and an “explore” phase, where the particle performs diffusionlike motion in a localized

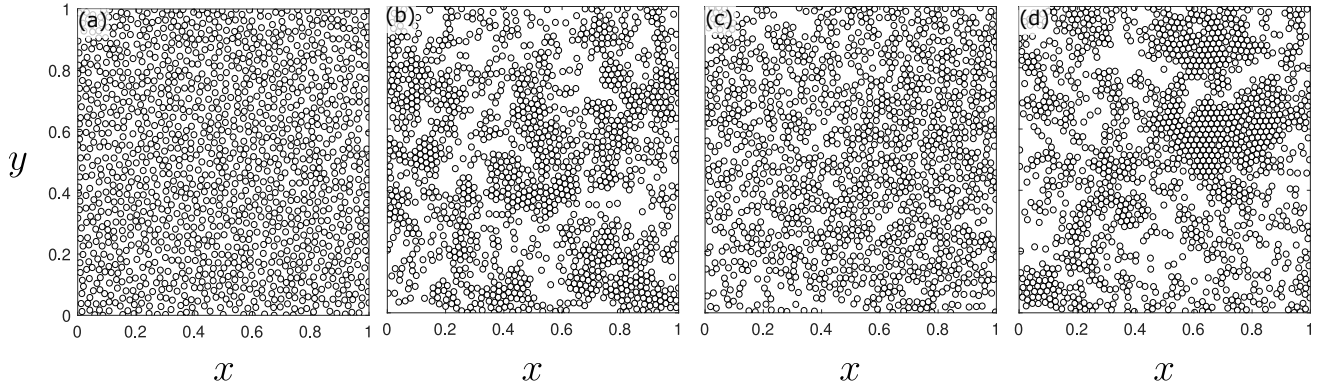


FIG. 7. Emergence of intermittent MIPS-like behavior when 1400 two-dimensional active particles driven by the Bouali attractor (see Fig. 6(e)-(h)) interact with each other via repulsive harmonic interactions (see also Supplemental Video S1). (a) ($t = 0$) Initially randomly located active particles in the “run” phase interact and result in (b) ($t = 46.9$) regions of high and low densities analogous to MIPS. (c) ($t = 187.5$) These particles then start switching their directions frequently during the “explore” phase, which results in the disintegration of clusters. (d) ($t = 312.5$) After some time, the particles again enter the long “run” phase and clusters form once more. This cycle keeps repeating as the phase-space trajectory evolves on the strange attractor. The parameters for the Bouali attractor are the same as in Fig. 6(e)-(h). The spring constant for the repulsive forces between the particles is $K = 50$ and the radius of each particle is 0.01. The particles were initiated at random locations in a unit-square periodic domain with slightly different initial conditions $((X(0), Y(0), Z(0)) = (-1, 1, 0) + \eta(t)$, where $\eta(t)$ is a random number selected uniformly from the interval $[0, 0.01]$.

region of space with relatively short run durations. The probability distribution of the time spent in ballistic motion clearly shows these two separate time-scales (see Fig. 6(g)) which is an imprint of the crossing statistics of the phase-space trajectory on the Bouali attractor with the specified cutting plane (see Fig. 6(h)). Another example employs a scaled Lorenz system with a Gaussian turning-angle distribution, to generate a 2D ABP-like particle (see Appendix E).

Instead of choosing the turning angle only at trigger times, one can choose the turning angle continuously from the driving strange attractor, e.g. using

$$\Delta\theta(t) = Z(t) \bmod(2\pi)$$

for the Lorenz strange attractor. This results in a curlicued trajectory with circular and spiral structures as shown in Fig. 6(i).

In this way, one can generate a diverse class of 2D active particle trajectories whose dynamics and statistics will be characterized by the choice of the underlying attractor, the cutting plane and the turning-angle selection rule.

2. Many interacting active particles

Active particles generally accumulate where they are moving slowly. This results in emergence of motility-induced phase separation (MIPS) where high-density and low-density phases are observed in a large collection of active particles¹⁴. In addition to generating conventional MIPS-like phenomena using our strange-attractor-driven framework (see Appendix E), we can also generate more exotic MIPS phenomena easily using our strange-attractor driving. For example, interactions of many active particles generated from the Bouali attractor⁶¹ (see Figs. 6(e)-(h)) results in intermittent

MIPS-like phenomena as shown in Fig. 7 and Supplemental Video S1. Since the Bouali-attractor driven active particle gives rise to a trajectory where the particle alternates between a long “run” phase and an “explore” phase, interactions of many such Bouali-attractor-driven particles via harmonic repulsive interactions (as described in Appendix B) result in cyclical emergent MIPS-like phases. The MIPS-like state is realized when the active particles are in the long “run” phase and we observe emergence of clusters. After some time, when the particles enter the “explore” phase, their diffusionlike motion results in the disintegration of clusters. This process repeats as particles alternate between the long “run” phase and the “explore” phase, and we obtain cyclical phases of MIPS-like clustered regions and gas-like phases with no clear large-scale structure.

By adding aligning interactions between 2D active particles in our formalism employing strange-attractor driving, we observe the emergence of complex flocking dynamics. This is illustrated in Fig. 8 and Supplemental Video S2. Here, each active particle is driven by the Lorenz attractor along with the cutting plane $X = 0$. To this, we add Vicsek-model-like aligning interactions¹² where each particle aligns itself based on the average direction of the particles in a neighborhood of radius Δ . In our model, each active particle gives weight W to the average alignment of its neighbors θ_{nb} and weight $1 - W$ to its own inherent angle θ_{own} arising from the driving strange attractor. Thus, the angle of the i th particle at time t_k evolves according to

$$\theta^i(t_k) = W\theta_{nb}^i(t_k) + (1 - W)\theta_{own}^i(t_k),$$

where

$$\theta_{nb}^i(t_k) = \tan^{-1} \left(\frac{\langle \sin(\theta(t_{k-1})) \rangle_{\Delta}}{\langle \cos(\theta(t_{k-1})) \rangle_{\Delta}} \right)$$

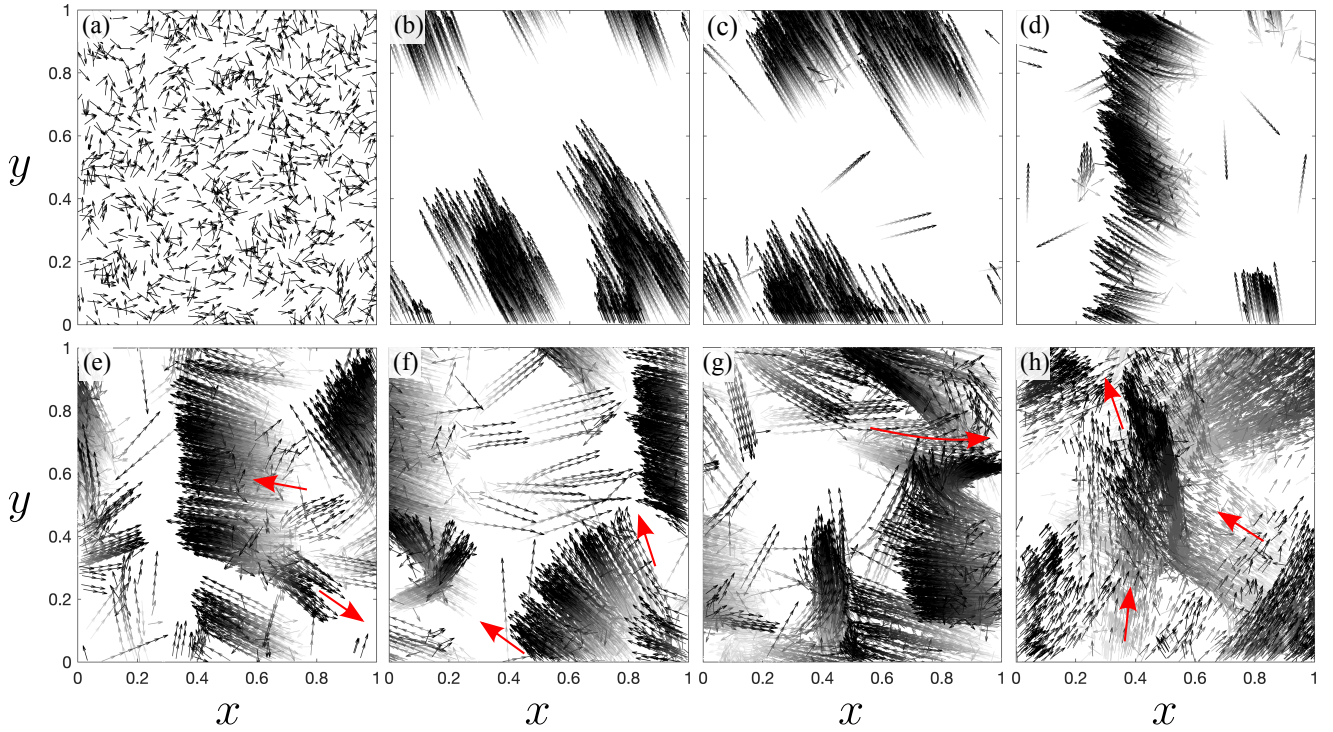


FIG. 8. Complex emergent dynamics in 2D flocking of strange-attractor-driven active particles on a periodic unit-square domain. 1000 Lorenz-attractor-driven active particles (as described in the caption to Fig. 6(a)-(b)) are initialized with random starting positions and directions, along with Vicsek-model-like aligning interactions, as described in the main text. The interaction radius of each particle is $\Delta = 0.05$ and the weight factor $W = 0.5$. (a) ($t = 0$) Initially randomly-located and randomly-oriented particles align and form (b) ($t = 5.2$) a coherent flocking phase at early times. At later times we observe more complex flocking dynamics such as (c) ($t = 11.8$) a few particles leaving the coherent flock, (d) ($t = 19.2$) deformation of the coherent flock into a banded structure, (e) ($t = 23.3$) spontaneous ejection of a smaller flock from a bigger flock, (f) ($t = 23.8$) flock expansion, (g) ($t = 26.1$) scattering of flocks and (h) ($t = 36.1$) merging of flocks. For an animated simulation see Supplemental Video S2. The color gradient in the grayscale level shows the past positions of the active particles, with the current position indicated in black. The self-propulsion speed of each particle is $u = 1$.

gives the average direction of particles (including particle i) within a circle of radius Δ , and

$$\theta_{\text{own}}^i(t_k) = \begin{cases} Z(t_k) & t_k = t_n \\ \theta^i(t_{k-1}) & \text{otherwise} \end{cases}$$

where t_n corresponds to trigger times and Z is the variable from the Lorenz system (see Appendix B for more details). An example of the complex flocking dynamics emerging from these interaction rules is shown in Fig. 8. Starting with 1000 active particles randomly positioned in a 2D periodic domain with random alignments, we initially obtain coherent motion as shown in Fig 8(b). Once the phase-space trajectory settles on the Lorenz attractor after an initial transient, particles start to leave the coherent flock (see Fig. 8(c)). This results in deformation and change in direction of the coherent flock (see Fig. 8(d)). Further evolution leads to several complex dynamical behaviors such as flock ejection (Fig. 8(e)), flock expansion (Fig. 8(f)), scattering of flocks (Fig. 8(g)) and merging of flocks (Fig. 8(h)). Moreover, by incorporating repulsive harmonic interactions in this system along with the Vicsek-like aligning interactions, we get the emergence of 2D motile crystalline clusters which show features such as void formation and persistence of alignment disturbances within a clus-

ter (see Supplemental Video S3), in addition to the features described in Fig. 8.

IV. DISCUSSION

It is common for elementary textbooks on classical mechanics to consider the dynamics of single point particles, subsequently generalizing to ensembles of interacting point particles. In either case, the state of the system may be specified using suitable generalized coordinates and their corresponding generalized velocities. Structure can be endowed upon the hitherto-structureless point particles via suitable internal degrees of freedom, e.g. Euler angles associated with each member of a swarm of rigid bodies. These additional internal degrees of freedom may be used to augment the system's generalized coordinates and generalized velocities. If a transition is then made from generalized velocities to canonically conjugate momenta, Hamilton's equations can be employed to study the evolution of the system⁶³.

For a single classical particle, or each member of a system of classical particles, we can augment the generalized coordinates and velocities (associated with degrees of freedom such

as position and mechanical momentum) with a generalized coordinate and velocity coupled to a driving strange attractor. The attractor component of the state space for each particle is an evolving vector $(X(t), Y(t), Z(t), \dots)$ which traces out a trajectory in the phase space \mathcal{S} , along a driving single-parameter strange attractor set $\mathcal{A} \in \mathcal{S}$. For example, consider an otherwise structureless point particle, having a single internal degree of freedom associated with a Lorenz attractor having fixed σ, r, b and fixed cutting plane $X = k$. An associated generalized coordinate, corresponding to the previously mentioned single degree of freedom associated with \mathcal{A} , is the arc length $s(t)$ (see Fig. 2 for a schematic) that corresponds to the length swept out by the state-space vector

$$\mathbf{R}(t) = (X(t), Y(t), Z(t)) \in \mathcal{A}.$$

The corresponding generalized velocity is $\dot{s}(t)$, namely the speed at which the attractor manifold \mathcal{A} is traversed. If it is meaningful to ascribe both kinetic and potential energies to the particle, a Lagrangian can be subsequently constructed, which in turn can be used to obtain the canonically conjugate momentum⁶³ corresponding to the strange-attractor degree of freedom s (see e.g. the article by Axenides and Floratos⁶⁴, which describes phase-space dynamics on a strange attractor in the framework of dissipative Nambu-Hamiltonian mechanics). This connection enables a higher-mechanics formalism similar to that of Hamilton and Lagrange to be employed, to study the spatiotemporal evolution of one or more particles (or extended bodies), that have a driving-strange-attractor degree of freedom in addition to standard degrees of freedom such as position, velocity, Euler angles, etc. Independently of whether or not a formalism akin to the canonical formalism of Hamilton and Lagrange can be employed, phase-space flows can be induced that are associated with the driving-attractor degree of freedom and its associated generalized velocity.

It is also worth commenting on rare trigger events, induced by the driving attractor \mathcal{A} and an associated cutting plane \tilde{P} . Such rare events occur over characteristic timescales that are very long, compared to the timescale T associated with a segment of the driving attractor that has a winding number on the order of unity (relative to an origin located at the “center of mass” of the segment). For example, for the Lorenz or Bouali attractors, T is of the order of the time taken to traverse one “loop” of a lobe. More generally, T may be defined as the characteristic time that a state-space trajectory would require, to traverse a state-space arc length $s(t+T) - s(t)$ that is on the order of the diameter \mathcal{D} of \mathcal{A} , provided that \mathcal{D} is finite. For example, suppose the driving attractor to be of the Lorenz type, with cutting plane $P \rightarrow \tilde{P}$ in Fig. 1 such that only a very small fraction $f \ll 1$ of the strange attractor’s measure lies to a particular side of \tilde{P} . This ensures that—for a generic starting point on \mathcal{A} —the probability of crossing \tilde{P} is extremely low, over a timescale on the order of the typical time T taken to traverse one loop of the Lorenz attractor. Such rare-event triggers could be used to model the finite lifetime of one or more interacting particles, in a variety of settings including the active-matter examples in the present paper. For example, in Fig. 1, the cutting plane P (which drives the active-particle dynamics), could be augmented with the rare-event cutting plane

\tilde{P} , which models the death (destruction, annihilation, absorption) of an active particle. A similar device could be used to model the birth (creation, emission) of an active particle.

Variants of our model could be examined, in which the driving strange attractor for each individual particle evolves with time, in a manner that is both deterministic and secular. For example, if we work with a driving attractor of the Lorenz type, the parameters $\sigma_m(t), r_m(t), b_m(t)$ for the m th particle could all be functions of time t that evolve according to a deterministic rule. This evolution of the driving attractor could be considered secular if its characteristic timescale is long compared to T . Moreover, a partitioning into equivalence classes may be induced by the secular evolution of each individual particle’s driving attractor. For example, given the set of cutting planes $\{P_m(t)\}$ —with one such cutting plane for each particle—the ensemble of particles is split into two equivalence classes $\mathcal{C}_1, \mathcal{C}_2$. These equivalence classes correspond to whether $P_m(t)$ does or does not intersect the secularly-evolving driving attractor $\mathcal{A}_m(t)$ of the m th particle. Stated more precisely, the m th particle is in \mathcal{C}_1 at time t if

$$\mathcal{A}_m(t) \cap P_m(t) \neq \emptyset,$$

where \emptyset denotes the null set, otherwise the m th particle is in \mathcal{C}_2 . If there are two or more cutting planes for each particle, the number of induced equivalence classes increases. Attractor-driven particles belonging to different equivalence classes may exhibit qualitatively different behavior, with individual particles changing equivalence class when a given cutting plane changes from having a null to a non-null intersection with the driving attractor, or vice versa. Note, also, that depending on the morphology of the attractor, additional equivalence classes may be induced because the set of all cutting planes that intersect the attractor may itself be dividable into natural classes. For example, for the Lorenz strange attractor, cutting planes in \mathcal{C}_1 may be divided into four disjoint subclasses: (i) cutting planes in subclass \mathcal{C}_{1a} that pass through the hole of the right-hand lobe in the half-space $X > 0$, but not through the other hole, as shown e.g. by the vertical red line in the lower panel of Fig. 5(a); (ii) cutting planes in subclass \mathcal{C}_{1b} that pass through the hole of the left-hand lobe, in the half-space $X < 0$, but not through the right-hand hole; (iii) cutting planes in subclass \mathcal{C}_{1c} that pass through both holes, as shown e.g. by the diagonal red line in the lower panel of Fig. 5(c); (iv) cutting planes in subclass \mathcal{C}_{1d} that intersect the attractor but pass through neither hole.

Further to the preceding paragraph, suppose that subsequent spatial coarse-graining is employed, so that the ensemble of attractor-driven particles can be viewed as a continuum field⁶⁵. In this context, it would be interesting to study if there is any correlation between (i) the different equivalence classes $\mathcal{C}_1, \mathcal{C}_2, \dots$, and (ii) different thermodynamic phases of the resulting multicomponent fluid⁶⁶. It might also be interesting to investigate the emergent equations of motion associated with the coarse-grained effective continuum field. Even in the absence of spatial coarse graining, the different equivalence classes may behave in a qualitatively different manner, corresponding to different populations of interacting particles, even

though the underlying attractor-driven model is by assumption the same for all particles.

We now turn to the question of how attractor-driven dynamics can be used to generate effective force fields, as functions of both position and time, in a manner that is directly induced by the driving attractors. Recall our earlier mention that the cutting plane P can be a specified function of position that is the same for all members of a swarm of attractor-driven particles. If this idea were to be applied to the particular example explored in Fig. 5(a), the cutting-plane field $P(x)$ in Eq. (5) could be used to channel active particles (and their associated coherent structures) in a position-dependent manner. The cutting-plane field can thereby induce a potential landscape $V(x)$ which influences the motion of the emergent clusters that move through it, by having a preferred direction of motion and preferred speed of motion that depends on x . By suitably extending the cutting-plane field to a specified function $P(x, t)$ of both position x and time t , namely by generalizing Eq. (5) to

$$a(x, t)X + b(x, t)Y + c(x, t) = 0,$$

an effective spatiotemporal landscape $V(x, t)$ could be induced. For example, cutting-plane fields could easily be devised that corral active particles within a specified region, before releasing them into a suitable potential landscape $V(x)$ or $V(x, t)$. In this manner, our model could be extended to study systems such as panicking crowds in stadia, traffic flow, disease transmission, ecosystem-invasion biology, swarming robots, etc. Moreover, the cutting-plane field could be a function of the discrete-particle index m , as well as the spacetime coordinates (x, t) .

Given the previous paragraph's description of how strange-attractor internal degrees of freedom can be coupled to an induced external applied field, it is natural to next consider how strange-attractor internal state-space manifolds may be coupled to one another, in the context of interacting neighboring particles. This can be done in a number of ways, and we here restrict consideration to two simple indicative examples. (i) At any time t , the respective internal states $\mathbf{R}_a(t) \in \mathcal{A}_a$ and $\mathbf{R}_b(t) \in \mathcal{A}_b$ of particles a and b may be used to generate an interaction potential

$$V'_{ab} = \varepsilon f(d_{ab}) \mathbf{R}_a(t) \cdot \mathbf{R}_b(t).$$

Here, ε is a real coupling constant and $f(d_{ab})$ is a scalar function of the separation $d_{ab} \geq 0$ between particles a and b . Typically, $f(d_{ab})$ would tend to a constant when d_{ab} becomes arbitrarily large. (ii) More generally, at any time t , the internal states of particles a and b may be used to form a two-body interaction potential

$$V''_{ab} = f(d_{ab}) \sum_{\mu\nu} \varepsilon_{\mu\nu} R_a^\mu(t) R_b^\nu(t).$$

Above, $\varepsilon_{\mu\nu}$ is a real rank-two tensor coupling, $f(d_{ab})$ is as defined previously, and the indices μ, ν each range over the state-space coordinates (X, Y, Z, \dots) , so that $R_a^1(t)$ is the X component of $\mathbf{R}_a(t)$, $R_a^2(t)$ is the Y component of $\mathbf{R}_a(t)$, etc.

We close this discussion by recalling that a number of coherent structures were observed to emerge in our simulations based on the strange-attractor-driven active-matter model, which invites an obvious comparison with the emergent structures observed in conventional active-matter models driven by noise. In addition to understanding the similarities in the emergent structures arising from both formalisms, it would be interesting to explore any differences, particularly when those differences can be attributed to the strange-attractor nature of the driving.

V. CONCLUSIONS

We presented a simple formalism for generating particles that are driven by strange attractors, and showed examples of some of the many phenomena it can model in the context of active matter. In one dimension, we showed that we can model active particles such as RTP-like motion by driving the active particle with the classic Lorenz system. By adding repulsive interactions between such particles we showed the emergence of clustering and jamming which can be controlled and manipulated by making simple modifications to the strange-attractor driving. In two dimensions, we were able to generate various active particle trajectories such as run-and-tumble, run-reverse-flick, intermittent and curlicued trajectories. By including interactions among 2D active particles, we showed rich emergent behaviors such as intermittent MIPS-like phenomena for particles with purely repulsive interactions, and complex flocking dynamics for particles with aligning interactions. We note that the active motions and emergent collective behaviors generated using this framework have imprinted in them signatures of the underlying strange-attractor driving.

Although we only explored overdamped particle dynamics in this work, inertia can easily be introduced in our strange-attractor-driven matter framework by adding a term proportional to particle acceleration in the dynamical equations of the particles. Moreover, we restricted our exploration to dry active matter where interactions between the active particles are not mediated by the surrounding medium. However, our formalism can also be extended to wet active matter by coupling the strange-attractor-driven particle dynamics with the dynamics of the surrounding medium. For example, in the original context of walking droplets from which the present work is inspired, multiple walkers interact with each other via their underlying wave fields. Introducing such wave-mediated interactions between our strange-attractor-driven particles may result in novel emergent behaviors.

Lastly, our formalism might also be applied more broadly, beyond the realm of active matter. The ability of the presented formalism to model complex behaviors in a simple way via the use of a driving strange attractor of a low-dimensional chaotic system, might find applications in fields such as economics and finance, robotics, chemistry, biology and physics.

CONFLICT OF INTEREST

The authors have no conflicts to disclose.

DATA AVAILABILITY STATEMENT

The data that support the findings of this study are available from the corresponding author upon reasonable request.

Appendix A: Transforming the walker's integro-differential equation into a Lorenz-like system of ODEs

Here we provide a derivation to transform the walker's integro-differential equation of motion into a system of ODEs that take the form of the Lorenz system. Consider the walker's integro-differential equation of motion,

$$\kappa \ddot{x} + \dot{x} = \frac{\beta}{2} \int_{-\infty}^t \sin(x(t) - x(s)) e^{-(t-s)} ds.$$

We denote the wave-memory force by

$$Y(t) = \frac{\beta}{2} \int_{-\infty}^t \sin(x(t) - x(s)) e^{-(t-s)} ds.$$

Differentiating $Y(t)$ with respect to time and using the Leibniz integration rule, we have

$$\begin{aligned} \dot{Y}(t) &= -\frac{\beta}{2} \int_{-\infty}^t \sin(x(t) - x(s)) e^{-(t-s)} ds \\ &\quad + \frac{\beta \dot{x}}{2} \int_{-\infty}^t \cos(x(t) - x(s)) e^{-(t-s)} ds \\ &= -Y(t) + XW(t), \end{aligned}$$

where $\dot{x} = X$ and

$$W(t) = \frac{\beta}{2} \int_{-\infty}^t \cos(x(t) - x(s)) e^{-(t-s)} ds.$$

Differentiating $W(t)$ with respect to time, we get

$$\begin{aligned} \dot{W}(t) &= \frac{\beta}{2} - \frac{\beta}{2} \int_{-\infty}^t \cos(x(t) - x(s)) e^{-(t-s)} ds \\ &\quad - \frac{\beta \dot{x}}{2} \int_{-\infty}^t \sin(x(t) - x(s)) e^{-(t-s)} ds \\ &= \frac{\beta}{2} - W(t) - XY(t). \end{aligned}$$

By making a change of variables

$$Z(t) = \frac{\beta}{2} - W(t),$$

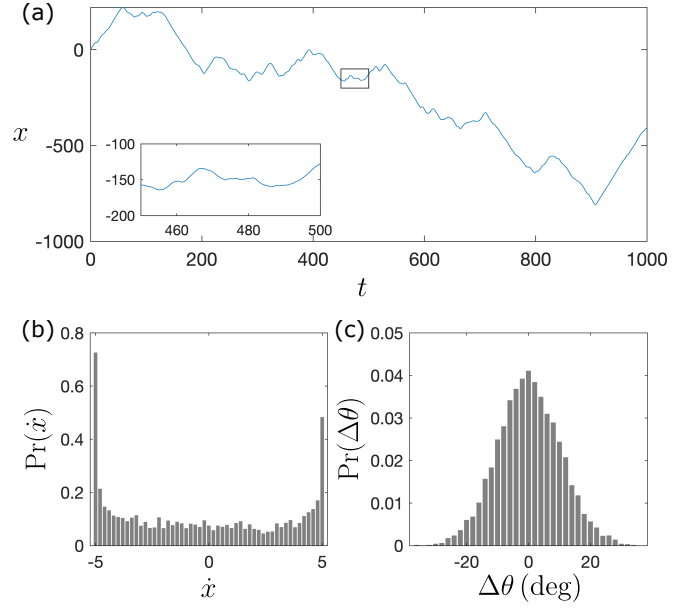


FIG. 9. Deterministic one-dimensional ABP-like particle generated from a scaled Lorenz system with parameters $\sigma = 10$, $r = 28$, $b = 8/3$ and $F = 10$. The one-dimensional trajectory of the particle is shown in (a), while (b) and (c) show the distribution of the particle velocity and the change-in-angle $\Delta\theta$ respectively. Here the constant speed $u = \sqrt{r-1}$. The mean of the Gaussian distribution for $\Delta\theta$ was chosen to be zero, while the standard deviation was chosen to be $\sigma_\theta = 10^\circ$.

we obtain the following system of Lorenz-like ODEs for the walker's dynamics:

$$\begin{aligned} \dot{x} &= X \\ \dot{X} &= \frac{1}{\kappa}(Y - X) \\ \dot{Y} &= -Y + \frac{\beta}{2}X - XZ \\ \dot{Z} &= -Z + XY. \end{aligned}$$

Appendix B: Details of numerical implementation

The simulation results presented in this paper were performed by first solving the chaotic dynamical system using the inbuilt ode45 solver in MATLAB and then coupling it with the particle's motion. We have attached example MATLAB codes in the Supplemental Material that simulate some of the behaviors presented in this manuscript. In this section, we provide more details for the implementation of the interactions between active particles.

1. Excluded-volume interactions for many particles in 1D

Excluded-volume interactions, leading to emergent phenomena in 1D for many interacting Lorenz-attractor-driven

RTP-like particles (as shown in Figs. 3 and 4 of the main text), were implemented as follows:

1. On the unit interval, with periodic boundary conditions, we define the distance d_{ij} between two particles i and j as the shortest distance between them:

$$d_{ij} = \min(|x_i - x_j|, 1 - |x_i - x_j|).$$

2. For each particle, we find the particles that are within a distance d , i.e. $d_{ij} < d$. Here, the distance d corresponds to the size of each particle.
3. For each such pair that are closer than the particle size, the motion ceases. However, their velocities continue to evolve on the strange attractor, so when a particle reverses its direction of motion and moves away from the other particle, the particle can resume its ballistic motion.

MATLAB code which implements these excluded-volume interactions for Lorenz-attractor-driven particles can be found in the file `oneD_many_particles.m`.

2. Aligning interactions for two-dimensional flocks

Aligning interactions, leading to the complex flocking dynamics in Fig. 8 of the main text, were implemented as follows:

1. For particles in the unit square with periodic boundary conditions, we define the shortest distance between the particles i and j as

$$d_{ij} = \sqrt{(X_{ij})^2 + (Y_{ij})^2},$$

where

$$\begin{aligned} X_{ij} &= \min(|x_i - x_j|, 1 - |x_i - x_j|), \\ Y_{ij} &= \min(|y_i - y_j|, 1 - |y_i - y_j|). \end{aligned}$$

2. For each particle, we define a neighborhood which is a circle of radius Δ . If there is no other particle inside this neighborhood, then the particle can continue to move as an individual active particle, driven by its strange attractor with its orientation $\theta_{\text{own}}(t)$.
3. If there are other particles in the neighborhood of the i th particle, then we use a weight factor W to determine the relative importance that the particle gives to the alignment of other particles, compared to its own directed motion driven by the strange attractor. Thus, the particle's orientation evolves according to

$$\theta_{\text{new}}(t) = W \theta_{\text{nb}}(t) + (1 - W) \theta_{\text{own}}(t).$$

Here θ_{nb} is the average direction of the particles in the neighborhood, defined in the same way as the Vicsek flocking model¹² and as given in Sec. III B of the main text.

MATLAB code which implements these aligning interactions for 2D Lorenz-attractor-driven particles can be found in the file `twoD_many_particles_flocking.m`.

Appendix C: One-dimensional active particles

1. Active Brownian Particles (ABPs) and Active Ornstein-Uhlenbeck Particles (AOUPs) from strange attractors

Using the formalism for generating one-dimensional RTP-like active particles described in Sec. III A of the main text, one can also generate an ABP-like particle in a deterministic way using strange attractors. The equation of motion obeyed by a one-dimensional ABP-like particle is⁶⁰

$$\dot{x} = u \cos(\theta(t)).$$

Here, u is a constant speed, and $\theta(t)$ is an internal angular co-ordinate which in conventional ABP undergoes rotational diffusion. In our framework, we let it evolve on a strange attractor. It is calculated at each time step using

$$\theta(t_{i+1}) = \theta(t_i) + \Delta\theta(t_i).$$

A trajectory is simulated on a scaled Lorenz strange attractor system given by

$$\begin{aligned} \dot{X} &= F(\sigma(Y - X)) \\ \dot{Y} &= F(-Y + rX - XZ) \\ \dot{Z} &= F(-bZ + XY), \end{aligned}$$

where F is a non-zero real number. The trigger times t_n are determined by the intersection of a phase-space trajectory along the scaled Lorenz attractor with the cutting plane $X = 0$. The change in the internal angular co-ordinate, $\Delta\theta(t_i)$, is either (i) zero if the trajectory on the Lorenz strange attractor does not cross the cutting plane $X = 0$ in the time interval between t_{i-1} and t_i , or (ii) we select a value of $\Delta\theta(t_i)$ from a Gaussian distribution with a mean of 0 and a standard deviation of σ_θ generated in a deterministic way (using the method described in Appendix D) if the trajectory intersects the cutting plane during the time interval between t_{i-1} and t_i . This gives an ABP-like motion in one dimension, whose internal angular co-ordinate undergoes rotational diffusion-like behavior with a Gaussian-like distribution. A typical trajectory for an ABP-like particle generated in this manner, together with its corresponding internal distribution of $\Delta\theta$, is shown in Fig. 9. We note that instead of using a prescribed Gaussian distribution for the internal angular co-ordinate, we can also choose an appropriate strange attractor and a cutting plane which will result in Gaussian-like statistics arising naturally from the underlying attractor.

In a similar way, we can construct a trajectory of an AOUP-like particle using the same scaled Lorenz strange attractor. The equation of motion of a conventional AOUP particle in one-dimension is⁶⁰

$$\tau \ddot{x} + \dot{x} = \sqrt{2\Delta_s} \xi(t).$$

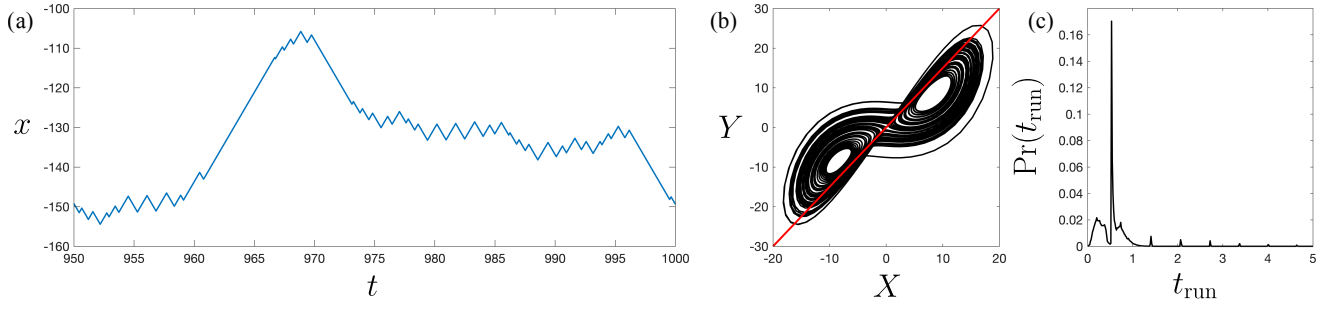


FIG. 10. One-dimensional Lorenz-strange-attractor-driven active particle with anomalous distribution of run durations. (a) Typical space-time trajectory. (b) The Lorenz attractor with parameters $\sigma = 10, r = 28, b = 8/3$ drives the active particle moving in one-dimension with a constant speed $u = \sqrt{r-1}$. The active particle reverses its walking direction when the state-space trajectory on the attractor crosses the $Y = 1.5X$ plane. (c) Probability distribution of time spent in constant-speed ballistic motion between direction reversals.

Here $\xi(t)$ is Gaussian white noise term with zero mean and unit variance, τ is a persistence-time constant and Δ_s is the strength of the noise term. By using the trigger times t_n of the scaled Lorenz system, we can generate an approximately Gaussian distribution using the process described in Appendix D, or select an appropriate strange attractor along with a cutting plane which results in a Gaussian-like distribution, which in the present context will be analogous to the noise term $\xi(t)$. Hence, we can create a trajectory for an AOUP-like particle in a deterministic manner, driven by strange attractors.

2. 1D RTP active particle with anomalous distribution of run durations

The Lorenz-attractor-driven RTP presented in Fig. 3 of the main text has an exponentially decaying envelope with discrete peaks in the probability distribution of run durations, which is analogous to the purely exponential distribution for a conventional RTP. However, we can also generate more diverse distributions of run durations for 1D active particles by changing the cutting plane and/or changing the underlying strange attractor. For example, as shown in Fig. 10, keeping the same parameters of the Lorenz strange attractor as Fig. 3 of the main text but choosing the cutting plane to be $Y = 1.5X$ results in an anomalous probability distribution of run durations, where the particle has frequent short run durations and occasional long run durations.

3. 1D motile clusters from strange attractors

In addition to jamming and cluster formation in one-dimension, as described in the main text, we can also generate one-dimensional motile clusters⁶⁰. This can be done by including harmonic repulsive interactions between the one-dimensional RTP-like particles, instead of the excluded-volume interactions used for Figs. 3 and 4 of the main text. We model the repulsive harmonic interactions between particles to activate when the distance between the particles falls

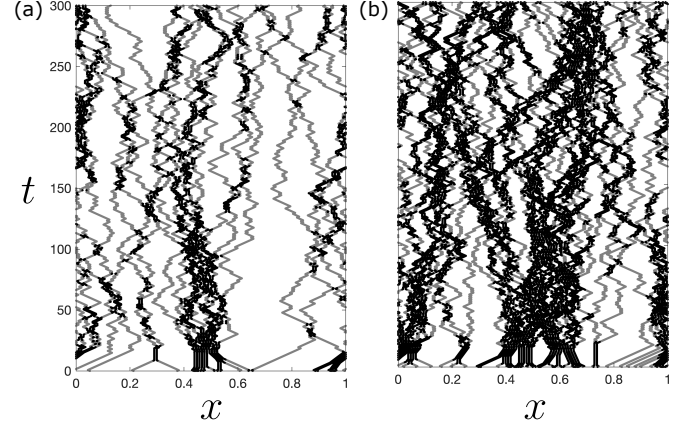


FIG. 11. 1D motile clusters resulting from harmonic repulsive interactions between RTP-like active particles driven by the Lorenz strange attractor. (a) Small motile clusters form which merge and disintegrate for a small number of particles $n = 20$, while (b) larger more persistent clusters form for a larger number of particles $n = 50$. Each particle has a speed of $u = 0.01$, spring interaction constant $K = 20$ and interaction distance $d_c = 0.005$. The Lorenz attractor parameters are $\sigma = 10, r = 28$ and $b = 8/3$. The gray trajectories denote isolated particles while the black trajectories denote clusters.

below a certain threshold $2d_c$, in which case the particles experience a repulsive force according to

$$F_{ij} = K \frac{x_i - x_j}{|x_i - x_j|} (2d_c - |x_i - x_j|).$$

We ensure that $|x_i - x_j|$ corresponds to the shortest distance between the particles in the periodic domain, and calculate the spring force accordingly. Figure 11 shows a typical output of simulations where these interactions are modeled between the RTP-like particles. We observe that for a small number of particles, we obtain small-sized transient motile clusters, while for a larger density of particles, we see larger long-lived motile clusters.

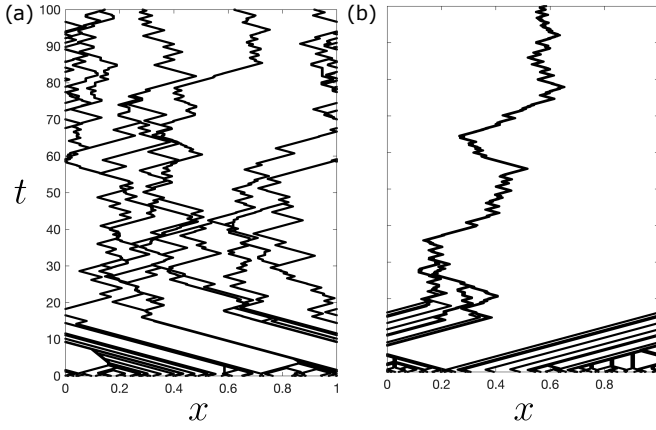


FIG. 12. 1D flocking behavior from aligning interactions of many RTP-like particles driven by the Lorenz strange attractor. (a) Small flocks form which merge and disintegrate for a small flocking-interaction neighborhood of $\Delta = 0.001$, while (b) a large single flock is formed for a large flocking-interaction neighborhood of $\Delta = 0.008$. The larger single flock in (b) also intermittently changes direction. Each particle has a speed of $u = 0.05$. The weight factor is $W = 0.9$, and the number of particles is 50. The Lorenz attractor parameters are $\sigma = 10$, $r = 28$ and $b = 8/3$.

4. 1D flocks from strange attractors

We can generate one-dimensional flocking behavior⁵⁹ by including aligning interactions for the one-dimensional RTP-like particles in a periodic domain. We implement the aligning interactions by allowing each such active particle to detect other active particles in a neighborhood of length Δ on either side of the particle. If there are no particles in the neighborhood, then the particle continues to evolve according to the RTP-like motion based on the Lorenz strange attractor. Conversely, if there are particles in the neighborhood then we sum the signs of the velocities of each of these particles (right as positive and left as negative) to find the direction of the majority of the particles in the neighborhood. For i th particle, this quantity is given by $\sum_{k \neq i} \text{sgn}(X_k)$. This quantity is then multiplied by a weight factor W and added to the product of the particle's own velocity direction $\text{sgn}(X_i)$ and the corresponding weight factor $1 - W$, giving us

$$T_i = W \sum_{k \neq i} \text{sgn}(X_k) + (1 - W) \text{sgn}(X_i).$$

Then $\text{sgn}(T_i)$ determines the direction of motion of the i th particle. A typical example of the observed flocking behavior is illustrated in Fig. 12. Here we observe that for a smaller flocking-interaction neighborhood size of $\Delta = 0.001$, we have small flocks while a larger flocking-interaction neighborhood of $\Delta = 0.008$ results in a single larger flock that erratically changes direction.

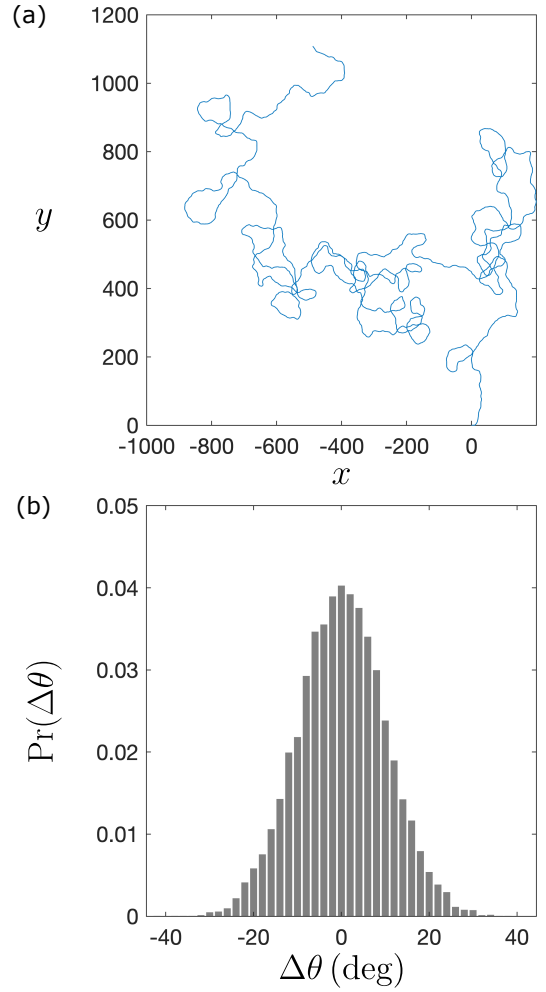


FIG. 13. Two-dimensional ABP-like particle generated from a scaled Lorenz system with parameters $\sigma = 10$, $r = 28$, $b = 8/3$ and $F = 10$. The trajectory of the particle is shown in (a), while (b) shows the probability distribution of the turning angle $\Delta\theta$. Here $u = \sqrt{r-1}$, the mean of the Gaussian distribution was chosen to be zero, and the standard deviation was chosen to be $\sigma_\theta = 10^\circ$.

Appendix D: Generating arbitrary turning-angle distributions deterministically

We can deterministically generate arbitrary probability distributions for turning angles, $\text{Pr}(\Delta\theta)$, using the trigger times t_n (see Fig. 1 of main text). Let

$$\alpha = \pi(\phi - 1),$$

where

$$\phi = (1 + \sqrt{5})/2$$

is the golden ratio. Now take the trigger times t_n , divide by a numerical time-step size Δt and round to the nearest integer, giving

$$S_n = \text{round}(t_n/\Delta t).$$

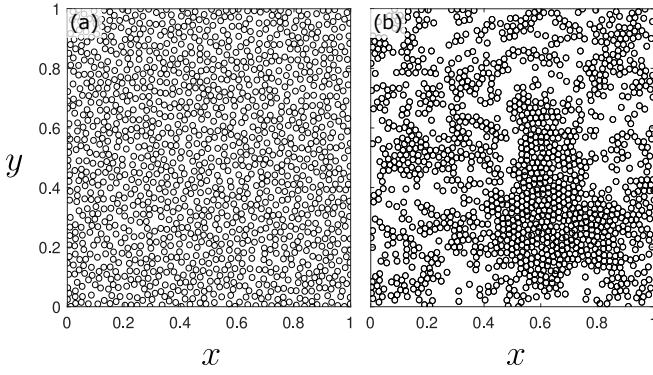


FIG. 14. Two-dimensional interactions of 1400 ABP-like particles resulting in MIPS (see also Supplemental Video S4). (a) Initial state of the system where particles are started randomly, within a unit square with periodic boundary conditions. (b) Emergence of MIPS, where regions of high density and low density are formed due to the repulsive interactions between the ABP-like active particles. The parameters for the ABP-like particles were the same as that described in Fig. 13. The spring constant for harmonic repulsive interactions was taken to be $K = 50$ and the radius of each particle is 0.01.

We then obtain an approximately uniform-distribution sampling of the turning angles $\Delta\theta_n$, using⁶⁷

$$\Delta\theta_n = S_n \alpha \bmod(2\pi).$$

We can use this approximately-uniform distribution to generate an arbitrary distribution $\text{Pr}(\Delta\theta)$, using the inversion method described in Chap. 3 of the book by Devroye⁶⁸. We start by discretizing the desired distribution, giving

$$P_i = \text{Pr}(\Delta\theta_i).$$

Now, consider laying all these P_i on a horizontal line in sequence as P_1, P_2, \dots , where the length of each line segment P_i is its value. We can now generate an approximately uniform distribution to select a value on this line segment of length $\sum_i P_i$, according to

$$R_n = S_n \alpha \bmod \left(\sum_i P_i \right).$$

We identify the line segment P_j corresponding to length R_n and sample the corresponding turning angle $\Delta\theta_j$. This allows us to deterministically sample numbers for an arbitrary distribution by using the trigger times t_n .

Appendix E: Two-dimensional ABPs and motility-induced phase separation (MIPS)

Similar to the one-dimensional ABP-like motion described in Appendix C 1, we can also deterministically generate a two-dimensional ABP-like trajectory for an active particle that is driven by the scaled Lorenz system. We use the same scaled Lorenz system as in Appendix C 1 and the same Gaussian distribution for the rotational diffusion. Implementing them with

the following equation for two-dimensional particle velocity

$$\begin{aligned} \dot{x} &= u \cos(\theta(t)) \\ \dot{y} &= u \sin(\theta(t)), \end{aligned}$$

we obtain a two-dimensional ABP-like trajectory as shown in Fig. 13. In conventional active matter, ABPs have been shown to undergo MIPS¹⁴. By exploring a large collection of two-dimensional ABP-like particles considered here, with added repulsive harmonic interactions as described in Sec. C 3 of the main text, we also obtain MIPS-like emergent behavior as shown in Fig. 14 and Supplemental Video S4.

- ¹Y. Couder, S. Protière, E. Fort, and A. Boudaoud, “Dynamical phenomena: Walking and orbiting droplets,” *Nature* **437**, 208–208 (2005).
- ²R. N. Valani, A. C. Slim, and T. Simula, “Superwalking droplets,” *Phys. Rev. Lett.* **123**, 024503 (2019).
- ³J. W. M. Bush and A. U. Oza, “Hydrodynamic quantum analogs,” *Rep. Prog. Phys.* **84**, 017001 (2020).
- ⁴A. U. Oza, R. R. Rosales, and J. W. M. Bush, “A trajectory equation for walking droplets: hydrodynamic pilot-wave theory,” *J. Fluid Mech.* **737**, 552–570 (2013).
- ⁵M. Durey, “Bifurcations and chaos in a Lorenz-like pilot-wave system,” *Chaos* **30**, 103115 (2020).
- ⁶R. N. Valani, A. C. Slim, D. M. Paganin, T. P. Simula, and T. Vo, “Unsteady dynamics of a classical particle-wave entity,” *Phys. Rev. E* **104**, 015106 (2021).
- ⁷E. N. Lorenz, “Deterministic nonperiodic flow,” *J. Atmos. Sci.* **20**, 130–141 (1963).
- ⁸Alternatively, or in addition, this attractor-induced trigger may signal the particle to select a corresponding variable based on non-attractor variables such as (i) the state of neighboring particles, and (ii) the potential landscape through which the particle moves.
- ⁹J. R. Howse, R. A. L. Jones, A. J. Ryan, T. Gough, R. Vafabakhsh, and R. Golestanian, “Self-motile colloidal particles: From directed propulsion to random walk,” *Phys. Rev. Lett.* **99**, 048102 (2007).
- ¹⁰S. Palagi and P. Fischer, “Bioinspired microrobots,” *Nat. Rev. Mater.* **3**, 113–124 (2018).
- ¹¹T. Vicsek and A. Zafeiris, “Collective motion,” *Phys. Rep.* **517**, 71–140 (2012).
- ¹²T. Vicsek, A. Czirók, E. Ben-Jacob, I. Cohen, and O. Shochet, “Novel type of phase transition in a system of self-driven particles,” *Phys. Rev. Lett.* **75**, 1226–1229 (1995).
- ¹³H. Chaté, “Dry aligning dilute active matter,” *Annu. Rev. Condens. Matter Phys.* **11**, 189–212 (2020).
- ¹⁴M. E. Cates and J. Tailleur, “Motility-induced phase separation,” *Annu. Rev. Condens. Matter Phys.* **6**, 219–244 (2015).
- ¹⁵T. Surrey, F. Nédélec, S. Leibler, and E. Karsenti, “Physical properties determining self-organization of motors and microtubules,” *Science* **292**, 1167–1171 (2001).
- ¹⁶F. J. Nédélec, T. Surrey, A. C. Maggs, and S. Leibler, “Self-organization of microtubules and motors,” *Nature* **389**, 305–308 (1997).
- ¹⁷V. Balakrishnan and S. Chaturvedi, “Persistent diffusion on a line,” *Physica A* **148**, 581–596 (1988).
- ¹⁸I. Bena, “Dichotomous Markov noise: Exact results for out-of-equilibrium systems,” *Int. J. Mod. Phys. B* **20**, 2825–2888 (2006).
- ¹⁹A. Dhar, A. Kundu, S. N. Majumdar, S. Sabhapandit, and G. Schehr, “Run-and-tumble particle in one-dimensional confining potentials: Steady-state, relaxation, and first-passage properties,” *Phys. Rev. E* **99**, 032132 (2019).
- ²⁰A. K. Hartmann, S. N. Majumdar, H. Schawe, and G. Schehr, “The convex hull of the run-and-tumble particle in a plane,” *J. Stat. Mech. Theory Exp.* **2020**, 053401 (2020).
- ²¹I. Santra, U. Basu, and S. Sabhapandit, “Run-and-tumble particles in two dimensions: Marginal position distributions,” *Phys. Rev. E* **101**, 062120 (2020).
- ²²P. Romanczuk, M. Bär, W. Ebeling, B. Lindner, and L. Schimansky-Geier, “Active Brownian particles,” *Eur. Phys. J. Spec. Top.* **202**, 1–162 (2012).
- ²³L. L. Bonilla, “Active Ornstein-Uhlenbeck particles,” *Phys. Rev. E* **100**, 022601 (2019).

- ²⁴B. J. Cole, “Is animal behaviour chaotic? Evidence from the activity of ants,” *Proc. Royal Soc. B* **244**, 253–259 (1991).
- ²⁵A. M. Reynolds, F. Bartumeus, A. Kölsch, and J. van de Koppel, “Signatures of chaos in animal search patterns,” *Sci. Rep.* **6**, 23492 (2016).
- ²⁶H. Miyoshi, Y. Kagawa, and Y. Tsuchiya, “Chaotic behavior in the locomotion of amoeba proteus,” *Protoplasma* **216**, 66–70 (2001).
- ²⁷T. Ahamed, A. C. Costa, and G. J. Stephens, “Capturing the continuous complexity of behaviour in *Caenorhabditis elegans*,” *Nat. Phys.* **17**, 275–283 (2021).
- ²⁸B. V. Hokmabad, R. Dey, M. Jalaal, D. Mohanty, M. Almukambetova, K. A. Baldwin, D. Lohse, and C. C. Maass, “Emergence of bimodal motility in active droplets,” *Phys. Rev. X* **11**, 011043 (2021).
- ²⁹C. Li, Y. Song, F. Wang, Z. Wang, and Y. Li, “A bounded strategy of the mobile robot coverage path planning based on Lorenz chaotic system,” *Int. J. Adv. Robot. Syst.* **13**, 107 (2016).
- ³⁰C. Nwachiona and J. H. Pérez-Cruz, “Analysis of a new chaotic system, electronic realization and use in navigation of differential drive mobile robot,” *Chaos Solit. Fractals* **144**, 110684 (2021).
- ³¹L. Moysis, E. Petavratzis, C. Volos, H. Nistazakis, and I. Stouboulos, “A chaotic path planning generator based on logistic map and modulo tactics,” *Robot. Auton. Syst.* **124**, 103377 (2020).
- ³²M. Rosalie, G. Danoy, S. Chaumette, and P. Bouvry, “Chaos-enhanced mobility models for multilevel swarms of UAVs,” *Swarm Evol. Comput.* **41**, 36–48 (2018).
- ³³V. Bacot, S. Perrard, M. Labousse, Y. Couder, and E. Fort, “Multistable free states of an active particle from a coherent memory dynamics,” *Phys. Rev. Lett.* **122**, 104303 (2019).
- ³⁴D. M. Harris, J. Moukhtar, E. Fort, Y. Couder, and J. W. M. Bush, “Wave-like statistics from pilot-wave dynamics in a circular corral,” *Phys. Rev. E* **88**, 011001 (2013).
- ³⁵G. Trefán, P. Grigolini, and B. J. West, “Deterministic Brownian motion,” *Phys. Rev. A* **45**, 1249–1252 (1992).
- ³⁶P. Gaspard, M. E. Briggs, M. K. Francis, J. V. Sengers, R. W. Gammon, J. R. Dorfman, and R. V. Calabrese, “Experimental evidence for microscopic chaos,” *Nature* **394**, 865–868 (1998).
- ³⁷C. Beck, “Dynamical systems of Langevin type,” *Physica A* **233**, 419–440 (1996).
- ³⁸L. Chew and C. Ting, “Microscopic chaos and Gaussian diffusion processes,” *Physica A* **307**, 275–296 (2002).
- ³⁹M. C. Mackey and M. Tyran-Kamińska, “Deterministic Brownian motion: The effects of perturbing a dynamical system by a chaotic semi-dynamical system,” *Phys. Rep.* **422**, 167–222 (2006).
- ⁴⁰R. Klages, *Microscopic chaos, fractals and transport in nonequilibrium statistical mechanics*, Advanced Series in Nonlinear Dynamics (World Scientific Publishing, Singapore, 2007).
- ⁴¹R. Festa, A. Mazzino, and D. Vincenzi, “Lorenz deterministic diffusion,” *Europhys. Lett. (EPL)* **60**, 820–826 (2002).
- ⁴²J. Lei and M. C. Mackey, “Deterministic Brownian motion generated from differential delay equations,” *Phys. Rev. E* **84**, 041105 (2011).
- ⁴³T. Albers, D. Müller-Bender, L. Hille, and G. Radons, “Chaotic diffusion in delay systems: Giant enhancement by time lag modulation,” *Phys. Rev. Lett.* **128**, 074101 (2022).
- ⁴⁴M. Hubert, S. Perrard, M. Labousse, N. Vandewalle, and Y. Couder, “Tunable bimodal explorations of space from memory-driven deterministic dynamics,” *Phys. Rev. E* **100**, 032201 (2019).
- ⁴⁵M. Durey, S. E. Turton, and J. W. M. Bush, “Speed oscillations in classical pilot-wave dynamics,” *Proc. Math. Phys. Eng. Sci.* **476**, 20190884 (2020).
- ⁴⁶M. Durey and J. W. M. Bush, “Classical pilot-wave dynamics: The free particle,” *Chaos* **31**, 033136 (2021).
- ⁴⁷R. N. Valani, “Anomalous transport of a classical wave-particle entity in a tilted potential,” *Phys. Rev. E* **105**, L012101 (2022).
- ⁴⁸G. M. Viswanathan, V. Afanasyev, S. V. Buldyrev, E. J. Murphy, P. A. Prince, and H. E. Stanley, “Lévy flight search patterns of wandering albatrosses,” *Nature* **381**, 413–415 (1996).
- ⁴⁹H. Löwen, “Inertial effects of self-propelled particles: From active Brownian to active Langevin motion,” *J. Chem. Phys.* **152**, 040901 (2020).
- ⁵⁰L. Angelani and R. Garra, “Run-and-tumble motion in one dimension with space-dependent speed,” *Phys. Rev. E* **100**, 052147 (2019).
- ⁵¹K. Malakar, V. Jemseena, A. Kundu, K. V. Kumar, S. Sabhapandit, S. N. Majumdar, S. Redner, and A. Dhar, “Steady state, relaxation and first-passage properties of a run-and-tumble particle in one-dimension,” *J. Stat. Mech. Theory Exp.* **2018**, 043215 (2018).
- ⁵²P. Singh and A. Kundu, “Generalised ‘arcsine’ laws for run-and-tumble particle in one dimension,” *J. Stat. Mech. Theory Exp.* **2019**, 083205 (2019).
- ⁵³P. Singh, S. Sabhapandit, and A. Kundu, “Run-and-tumble particle in inhomogeneous media in one dimension,” *J. Stat. Mech. Theory Exp.* **2020**, 083207 (2020).
- ⁵⁴L. Angelani, R. Di Leonardo, and M. Paoluzzi, “First-passage time of run-and-tumble particles,” *Eur. Phys. J. E* **37**, 59 (2014).
- ⁵⁵L. Angelani, “Confined run-and-tumble swimmers in one dimension,” *J. Phys. A Math. Theor.* **50**, 325601 (2017).
- ⁵⁶N. Sepúlveda and R. Soto, “Coarsening and clustering in run-and-tumble dynamics with short-range exclusion,” *Phys. Rev. E* **94**, 022603 (2016).
- ⁵⁷R. Dandekar, S. Chakraborti, and R. Rajesh, “Hard core run and tumble particles on a one-dimensional lattice,” *Phys. Rev. E* **102**, 062111 (2020).
- ⁵⁸R. Soto and R. Golestanian, “Run-and-tumble dynamics in a crowded environment: Persistent exclusion process for swimmers,” *Phys. Rev. E* **89**, 012706 (2014).
- ⁵⁹O. J. O’Loan and M. R. Evans, “Alternating steady state in one-dimensional flocking,” *J. Phys. A Math. Gen.* **32**, L99–L105 (1999).
- ⁶⁰P. Dolai, A. Das, A. Kundu, C. Dasgupta, A. Dhar, and K. V. Kumar, “Universal scaling in active single-file dynamics,” *Soft Matter* **16**, 7077–7087 (2020).
- ⁶¹S. Bouali, “A 3D strange attractor with a distinctive silhouette. The butterfly effect revisited,” (2014), arXiv:1311.6128.
- ⁶²J. Taktikos, H. Stark, and V. Zaburdaev, “How the motility pattern of bacteria affects their dispersal and chemotaxis,” *PLoS ONE* **8**, e81936 (2013).
- ⁶³H. Goldstein, *Classical Mechanics*, 2nd ed. (Addison-Wesley Publishing Company, Reading, Massachusetts, 1980).
- ⁶⁴M. Axenides and E. Floratos, “Strange attractors in dissipative Nambu mechanics: classical and quantum aspects,” *J. High Energy Phys.* **2010**, 36 (2010).
- ⁶⁵J. Toner and Y. Tu, “Long-range order in a two-dimensional dynamical XY model: How birds fly together,” *Phys. Rev. Lett.* **75**, 4326–4329 (1995).
- ⁶⁶M. J. Bowick, N. Fakhri, M. C. Marchetti, and S. Ramaswamy, “Symmetry, thermodynamics, and topology in active matter,” *Phys. Rev. X* **12**, 010501 (2022).
- ⁶⁷A. M. Kingston, D. Pelliccia, A. Rack, M. P. Olbinado, Y. Cheng, G. R. Myers, and D. M. Paganin, “Ghost tomography,” *Optica* **5**, 1516–1520 (2018).
- ⁶⁸L. Devroye, *Non-Uniform Random Variate Generation* (Springer-Verlag, 1986).